Nonlinear curve fit analysis for Acid blue 92 removal using functionalized carbon nanotubes

R. Siddharthan, P. Mahalingam*, P. Sivakumar, A. Loganathan

Department of Chemistry, Arignar Anna Government Arts College, Namakkal, Tamil Nadu – 637002, India,
emails: ponmahanano@gmail.com (P. Mahalingam), siddharth83.chem@gmail.com (R. Siddharthan), shivagobi@gmail.com
(P. Sivakumar), loghunadan@gmail.com (A. Loganathan)

ABSTRACT

Since functionalized carbon nanotubes exhibit enhanced surface chemistry, in this work, boron, nitrogen and sulfur doped carbon nanotubes were prepared through microwave process by treating the oxidized multi-walled carbon nanotubes with appropriate precursors. The carbon nanotubes were characterized using scanning electron microscopy, X-ray diffraction, Raman and Fourier-transform infrared spectroscopy. The study indicated that the functionalized carbon nanotubes with thickness of 50–60 nm retained their structure even after microwave process by showing rather smooth outer surface with I_D/I_G ratio range 0.6–1.2. Co-doping of boron, nitrogen and sulfur on the carbon nanotube layer enhanced the adsorption property. The functionalized carbon nanotubes were evaluated for its adsorption property to remove Acid blue 92 (AB92) from aqueous solution. The kinetics of AB92 adsorption was evaluated using linear and nonlinear mathematical models. Increase in temperature favours the AB92 adsorption on to the adsorbents prepared was supported by Gibbs free energy values (–3 to –10.8 kJ mol⁻¹). The thermodynamic parameters substantiate that the adsorption of AB92 onto these adsorbents is more favourable. The adsorbents were effective in removing AB92 at pH 6 following Freundlich isotherm with mass transfer of 1.995 mg g⁻¹ min⁻¹. The recyclability tests showed that the spent adsorbents were effective with 90% adsorption for up to 7 cycles.

Keyboards: Nonlinear model; Carbon nanotubes, B-N-S co-doped CNT; Microwave; Adsorption

1. Introduction

Carbon nanomaterials are known for their unique properties which are attributed to quantum effect, high surface area and single element material [1]. The unique properties of carbon nanotubes depend on its morphology, structure, defects. Defects in carbon nanotubes surface can be created by several methods but doping is a novel and controllable technique. Carbon nanotubes can be doped with both metal and nonmetals. Though the doped carbon nanotubes are used for various applications, using it for environmental remedies has become a trend of research [2,3]. Various methods are adopted by researchers to dope carbon nanotubes. However, utilization of multi steps or hazardous raw materials in these processes necessitates development of new approaches. Liu et al. [4] successfully doped multi hetero atoms on the surface of carbon nanotubes by simply coating multi-walled carbon nanotubes (CNTs) with polydopamine as an anchor for elements N, S and B. Kamran and Park [5] have demonstrated microwave-assisted, acid-functionalized carbon nanofibers decorated with manganese-doped titanium nanotubes for Li⁺ adsorption. Kumar et al. [6] employed co-precipitation method to synthesis Ag doped MnO_2-CNT nanocomposite and used as an effective adsorbent for elimination of Acridine Orange dye. The

* Corresponding author.

foregoing discussion reveals that doped carbon nanotubes could be an effective adsorbent for wastewater treatment. Since the adsorption properties of CNTs are linked to the delocalised electrons, obviously any elements with Lewis properties can tune the properties of carbon nanotubes. The industrial effluents normally contain synthetic dyes which invariably contain unsaturated or conjugated Pi bonds in its structure. Therefore, to tune the properties of carbon nanotubes, doping the outer surface with elements like N, B, S and their combinations by any green method is appropriated for environmental concern. The damage caused by the industrial dye effluent (Acid blue 92) in water bodies such as dark coloration, turbidity and partial degradation under sunlight decreases quality of water by reducing dissolved oxygen and altering pH level [7,8]. Also the complex organic dye molecules pose serious health issues to human beings, especially children. The dye molecules are carcinogenic, toxic and mutagenic as well [9]. Owing to the non-biodegradable nature, the dyes particularly azo dyes bio accumulates in the food chain and it is bio amplified at the top of the food chain [9]. The soil microbes are also affected by the azo groups of the dyes [10]. The removal of dyes in wastewater is highly warranted in the present scenario. There are plenty of methods available for the dye removal from its effluent. But adsorption using high surface materials is a promising one owing to its simplicity and wide selectivity. There are many materials like nano-carbon based adsorbents [11], chemically modified bagasse [12], MnNPs [13] were successfully tried for scavenging the dye molecules in aqueous medium. Though there are plenty of materials and methods available for dye removal, still a lot of scope is there to find low cost and environmentally friendly materials.

Moreover, characterizing physico-chemical properties of these materials and evolving kinetic and thermodynamic parameters for its adsorption property would be useful for better understanding and further tuning its properties for its effective use in environmental remedies. The present study aims to evaluate the effectiveness of carbon nanotubes to remove Acid blue 92 (AB92) from aqueous solution. The kinetics of a AB92 adsorption under various concentrations and temperatures are evaluated using linear and nonlinear mathematical models. The thermodynamic parameters are studied to substantiate the adsorption of AB92 onto these adsorbents.

2. Material and methods

2.1. Preparation and functionalization of CNTs

Following the procedure described by Kanagaraj et al. [14], the carbon nanotubes are prepared by spraying the precursor pine oil on silica supported Fe–Co–Ni catalyst at 650°C. The carbon nanotubes prepared are refluxed with 2N nitric acid followed by washing several times using deionised water to leach out metallic and other impurities. The oxidized carbon nanotubes are mixed with boric acid (MWCNT-B), boric acid, urea mixture (MWCNT-BN) and boric acid, thiourea mixture (MWCNT-BNS). The mixture is ground well using mortar and pestle. The mixture taken in a silica crucible is kept inside the domestic microwave oven and flushed with argon before microwave treatment. The mixture is microwave irradiated with 800 W for 20 min.

To get uniform irradiation, the mixture is stirred for every 2 min radiation exposure. Different compositions of precursors and carbon nanotubes are studied to optimize the doping process. A typical optimum condition of 0.2 g precursor and 1 g oxidized carbon nanotubes are used in the experiment. The functionalized material obtained after microwave treatment is ground well using mortar and pestle and washed several times using warm water centrifugation process, till the soluble materials are completely washed out. The residue material is dried in an air oven at 110°C and used for characterization and applications.

2.2. Adsorption analysis of AB92

All the reagents like HCl, NaOH (Analytical Grade) are purchased from Sigma-Aldrich, India. Acid blue 92 (AB92) dye (CI No.: 13390), Molecular Formula: $C_{26}H_{16}N_3Na_3O_{10}S_3$ and a molecular weight of 695.59 g mol^{-1} is chosen as a representative dye for the adsorption analysis using the selected sorbents. Throughout the analysis, double distilled water is used for the preparation and dilutions of dye solutions. A stock dye solution of 1,000 mg L^{-1} is prepared by dissolving the appropriate amount of AB92 dye (based on percentage purity) using double distilled water. Dye solutions with lower concentration are prepared by diluting the stock dye solution using double distilled water. The dye has one azo group and also contains three sulfonic acid groups.

2.3. Batch mode AB92 adsorption

The prepared nano-materials MWCNT-B, MWCNT-BN and MWCNT-BNS are used as adsorbent for their affinity towards AB92 dye. For the study of pH influence on dye adsorption, 100 mL of 50 mg L^{-1} AB92 solution is agitated with 100 mg of individual adsorbent and the residual dye concentration is evaluated using the optical density at the λ_{max} of AB92 dye (570 nm). For the dye concentration measurements Bio UV–Visible spectrometer (Elico make BL-198) is used. During the kinetic studies, dye solution of specified concentration (25, 50, 75 and 100 mg L^{-1}) is shaken with 100 mg CNTs, an aliquot of the mixture is withdrawn and analysed for residual AB92 concentration. The same studies are also performed under varying temperatures.

Isotherm studies are also performed to evaluate the adsorption mechanism. For the adsorption isotherm, varying concentration dye solutions are agitated with 100 mg of CNTs until the attainment of equilibrium (120 min). It is essential to perform the reusability studies to make the adsorbent as an economically beneficial one. The adsorbents are shaken with distilled water of various pH (using dil HCl and aq. NaOH), the dye removed by the eluent also estimated using photocalorimetric method, which is employed for adsorption studies.

3. Results and discussion

3.1. Characterization of adsorbents

3.1.1. Electron microscopic analysis

The oxidized carbon nanotubes treated with boric acid (MWCNT-B), boric acid, urea mixture (MWCNT-BN) and

boric acid, thiourea mixture (MWCNT-BNS) under microwave irradiation are characterized using scanning electron microscopy (SEM) technique. The SEM image of the prepared MWCNT-B, MWCNT-BN and MWCNT-BNS are depicted in Fig. 1.

The morphology of the products is analyzed for appearance, size and shape of the carbon nanotubes. The carbon nanotubes average size found for MWCNT-B, MWCNT-BN and MWCNT-BNS are 60, 54 and 58 nm respectively. The carbon nanotubes outer surface is found to be rather smooth in all the three samples. Fig. 1a reveals that boron doped multi-walled carbon nanotubes have nearly smooth surfaces without adherence of amorphous carbon or precursor materials. The smooth surface of MWCNT-B is attributed to lesser disorder created through doping of boron atoms in the carbon lattice during microwave treatment. The SEM images of MWCNT-BN and MWCNT-BNS are shown in Fig. 1b and c respectively. Fig. 1b shows a rather smooth surface of carbon nanotubes which is formed due to doping of boron and nitrogen. The carbon nanotubes treated with boron and thiourea are found to be with more bends and cracks (Fig. 1c). This may be attributed to the effective functionalization of carbon nanotubes surface with boron, nitrogen and sulphur.

3.1.2. X-ray diffraction analysis

The X-ray diffraction (XRD) pattern recorded for MWCNT-B, MWCNT-BN and MWCNT-BNS are shown in Fig. 2a. The XRD pattern (Fig. 2a) is used to infer the structure and crystalline nature of the prepared materials. Invariably all the prepared samples show 2θ peaks around 26.3, 44.7, 54.0, and 65.0 which is similar to the peaks generally observed for graphite structure. These results show that the functionalized MWCNTs retain their structure even after microwave treatment. The inter-planar distance calculated for these materials is found to be around 0.35 nm. However, the appearance of the characteristic 2θ peak corresponding to 002 planes for MWCNT-BNS is slightly shifted to a longer angle with increased inter-planar distance and full width half maximum as compared to MWCNT-B and MWCNT-BN. This is attributed to the sulfur doping as well as functionalization of the sidewall of the MWCNTs.

3.1.3. Raman spectrum analysis

The Raman spectrum of MWCNT-B, MWCNT-BN and MWCNT-BNS are shown in Fig. 2b. The Raman scattering of the prepared materials shows characteristic peaks around 1,342, 1,578 and 2,658 cm^{-1} which are similar to the peaks observed for graphitic layers. It is found that relative intensities of D band (characteristic of disorder) to G band (characteristic for crystalline), I_D/I_G, for the B-MWCNTs, BN-MWCNTs and BNS-MWCNTs are 0.6, 1.2 and 0.8 respectively. The higher value of I_D/I_G for MWCNT-BN indicates that the D peak intensity is higher than that of G peak and the corresponding material contains more disordered carbon structure. It is inferred from the I_D/I_G values of the
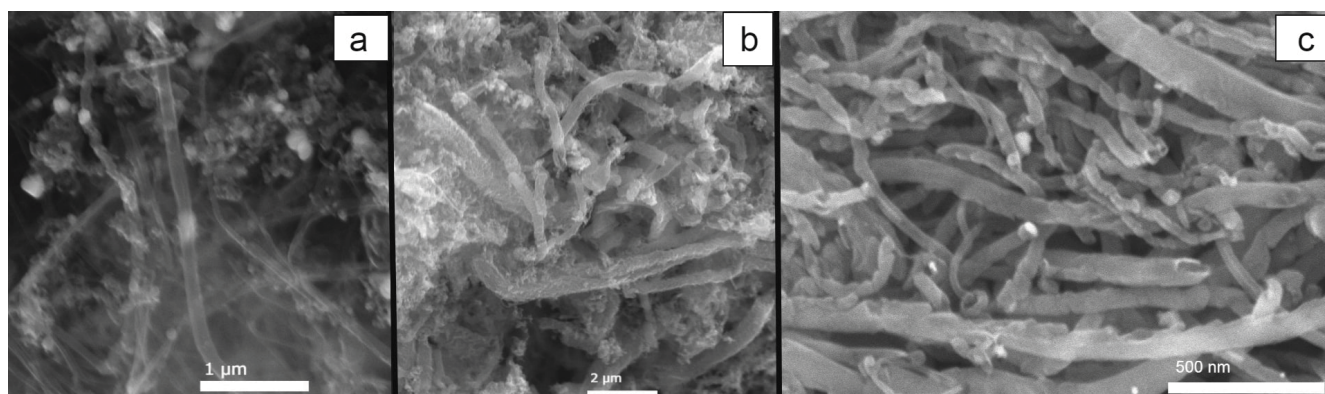

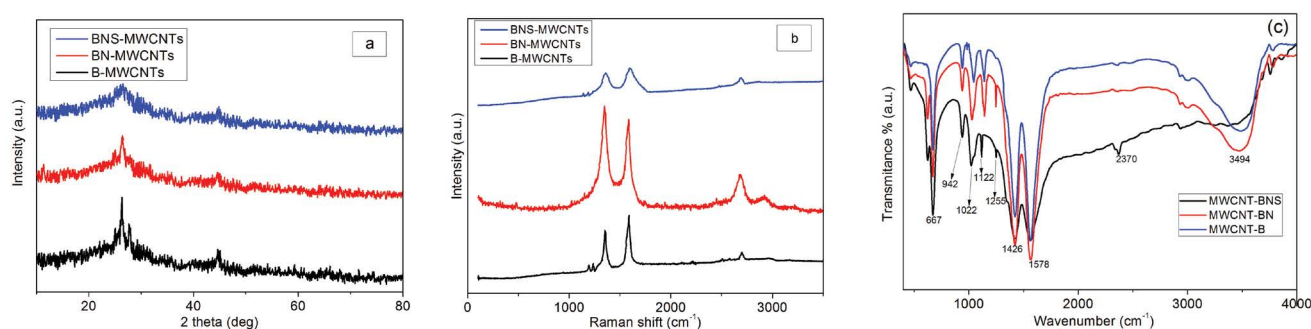Fig. 1. SEM image of (a) MWCNT-B, (b) MWCNT-BN and (c) MWCNT-BNS.

Fig. 2. (a) XRD pattern, (b) Raman spectrum and (c) FTIR spectrum of MWCNT-B, MWCNT-BN and MWCNT-BNS.

prepared materials that due to functionalization, the outer layer structure of MWCNTs is more distorted. The broadening and shifting of the G band of MWCNT-BNS to longer wave number indicates the disorder of the structure due to sulfur atom doping.

3.1.4. Fourier-transform infrared spectrum analysis

Fig. 2c shows the Fourier-transform infrared (FTIR) spectrum in the range 400–4,000 cm^{-1} of doped MWCNT. The broad peak at 3,494 cm^{-1} shows the presence of alcoholic or carboxylic OH and adsorbed water, while the intense peak at the peaks at 1,022 (O–B), 1,122 (C–B), 1,255 (C–N) and 1,426 (C–S) cm^{-1} indicates the doping of B, N and S in the carbon skeleton. The un-oxidized aromatic ring with distorted structure is indicated by the peak around 1,561. The peak around 1,448 cm^{-1} is ascribed to C–N stretching [15,16].

3.1.5. Surface parameters

The surface parameters like surface area, pore volume and pore size were estimated using N$_2$ adsorption–desorption isotherm using ASAP 2020 Gas sorption analyser. Samples were degassed at 12 h before the determination of surface area, pore volume and pore diameter. It was observed that the surface area of the prepared adsorbents MWCNT-B, MWCNT-BN and MWCNT-BNS are 64.82, 69.34 and 73.42 m^2 g^{-1} respectively. The MWCNT-BNS adsorbent has slightly higher surface area due to increased entanglement of CNTs and elevated heterogeneity [17]. The pore volume of MWCNT-B, MWCNT-BN and MWCNT-BNS are 0.1412, 0.1414 and 01479 cm^3 g^{-1} and the pore size of MWCNT-B, MWCNT-BN and MWCNT-BNS are 10.325, 10.718 and 11.323 nm respectively. The higher pore volume and pore size observed for MWCNT-BNS, could favour the increased uptake of AB92.

3.2. Adsorption studies

The adsorption properties of Acid blue 92 (AB92) from aqueous solution onto doped multi-walled carbon nanotubes are studied as a function of pH, initial AB92 concentration and temperature. Also, Langmuir and Freundlich isotherms and kinetic models are applied to fit the experimental data. Mechanism and thermodynamic parameters of AB92 adsorption onto doped MWCNTs are discussed.

3.2.1. Effect of pH on AB92 adsorption

The aqueous dye solution predominantly exists in the ionized form. The extent of adsorption of the ionized dye species depends primarily on the solution pH. The variation of AB92 dye adsorption as a function of pH by the selected adsorbents is evaluated by varying the solution pH from 2 to 10. The change in adsorption with respect to pH is graphically shown in Fig. 3. The selected dye AB92 is an anionic dye and in aqueous solution it ionizes as:

$$AB92 \rightleftharpoons \left[AB92 \right]^{3-} + 3Na^+$$

The pKa value of AB92 dye is 3.2, at lower pH, the dye ionization is minimum and leads to more Vander Waals adsorption with poor ionic interactions [18].The adsorption of ionized solutes on the solid surface occurs due to the combined effect of the charges on the solute as well as the charges on sorbent surface. At lower pH, the surface of CNTs is highly protonated, leading to high positive charge on CNTs surface. The positively charged CNTs show an excellent affinity towards the AB92 dye molecules. When the pH exceeds the zero point charge of CNT, the surface of sorbent is negative. The pH$_{ZPC}$ of MWCNT-B, MWCNT-BN and MWCNT-BNS are 6.4, 6.4 and 6.5 respectively. When the solution pH goes beyond 6.5, the surface of MWCNTs acquires a negative charge. The negatively charged CNTs show an electrostatic repulsion towards the dye and hence the quantity of AB92 adsorption decreases.

As observed from Fig. 3, the adsorption of AB92 onto MWCNT-B, MWCNT-BN and MWCNT-BNS increases up to a pH 6.0. When the pH exceeds 6.0, invariably all the three adsorbents show a decreased adsorption towards AB92.
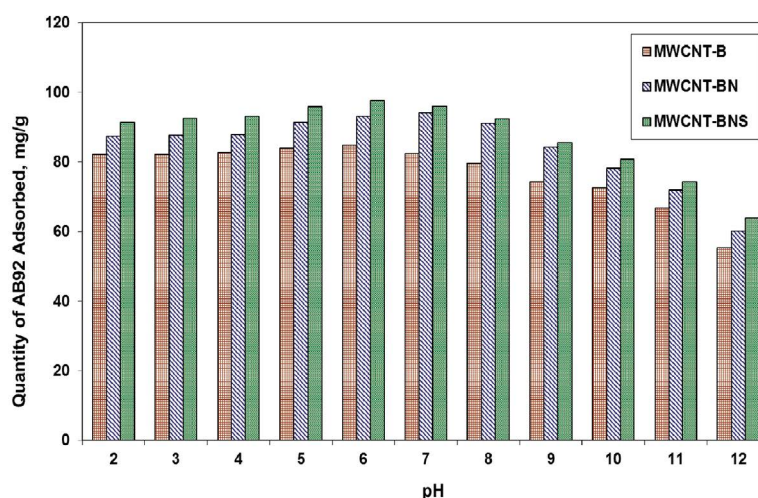

Fig. 3. Effect of pH on AB92 adsorption.

In order to implement the adsorption system in a large level industrial treatment process, it is essential to optimize the effluent pH under 7.0. The maximum uptake of AB92 at a pH of 6.0 was found to be 84.7, 93.2 and 97.7 mg g^{-1} for MWCNT-B, MWCNT-BN and MWCNT-BNS respectively. Among the three sorbents, MWCNT-BNS showed highest adsorption capacity due to the energetically favoured surface created by the BNS doping.

3.2.2. Effect of initial AB92 concentration

The impact of initial AB92 concentration on its affinity towards prepared nanoadsorbents is studied by altering the initial AB92 concentration from 25 to 100 mg L^{-1}. The variations of AB92 adsorption by the selected adsorbents under different concentrations are graphically provided in Fig. 4. While increasing the AB92 concentration from 25 to 100 mg L^{-1}, the percentage of AB92 removed through adsorption decreases from 87.10 to 78.15 for MWCNT-B, 95.16 to 88.70 for MWCNT-BN and 100 to 94.12 for MWCNT-BNS respectively. Though the percentage of dye removal decreases with increase of initial dye concentration, the quantity of AB92 removal per gram of adsorbent increases from 43.55 to 156.30 for MWCNT-B, 47.58 to 177.40 for MWCNT-BN and 50 to 188.24 for MWCNT-BNS respectively on increasing the initial AB92 concentration from 25 to 100 mg L^{-1}.

The rate of mass transfer is very fast during the first 40 min, the rate of sorption during the first 40 min is 1.755, 1.935 and 1.995 mg g^{-1} min^{-1} for MWCNT-B, MWCNT-BN and MWCNT-BNS respectively for a fixed AB92 concentration of 50 mg L^{-1}. The rate of adsorption slowly decreases with the time after 40 min and it reaches equilibrium at 110 min for all the three selected adsorbents under all the ranges of initial AB92 concentrations. The maximum quantity of AB92 removed at equilibrium was observed for an initial AB92 concentration of 100 mg L^{-1}. The doping of CNT's

surface with B, N and S energetically favours the solute adsorption [19]. Among the three variants, MWCNT-BNS showed maximum adsorption capacity towards AB92.

3.3. Adsorption kinetics

The rate of variation of mass transfer of solute from solution to sorbent is studied with the help of pseudo-first-order and pseudo-second-order mathematical expressions. Few decades back computational facilities were not available, hence, people used to linearize the mathematical expression for data analysis. Linearization of mathematical expressions can give results associated with errors [20]. Recently many software tools are available for data analysis using nonlinear mathematical expressions with minimum error. In the present study the kinetics of a AB92 adsorption under various concentrations and temperatures are evaluated using linear and nonlinear mathematical models. The nonlinear curve fit analysis is performed using Excel Solver tool available in Microsoft Excel 2010. The linear and nonlinear forms of kinetic expressions are given as follows [21,22].

Linear form of pseudo-first-order model:

$$\ln\left(q_e - q_t\right) = \ln q_e - k_1 t \qquad (1)$$

Nonlinear form of pseudo-first-order model:

$$q_t = q_e\left(1 - \exp^{-k_1 t}\right) \qquad (2)$$

Linear form of pseudo-second-order model:

$$\frac{t}{q_t} = \frac{1}{k_2 q_e^2} + \frac{1}{q_e} t \qquad (3)$$
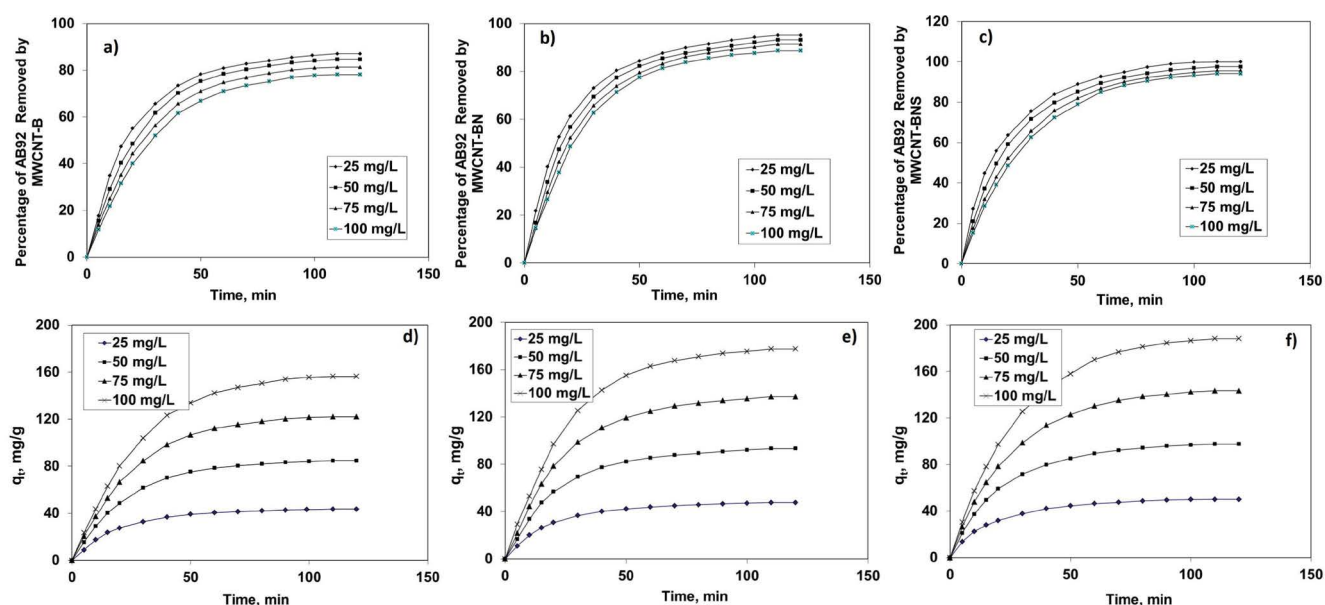

Fig. 4. Percentage of AB92 adsorption (a) MWCNT-B, (b) MWCNT-BN, (c) MWCNT-BNS and amount of AB92 adsorption (d) MWCNT-B, (e) MWCNT-BN and (f) MWCNT-BNS at various initial concentrations.

Nonlinear form of pseudo-second-order model:

$$q_t = \frac{k_2 q_e^2 t}{1 + k_2 q_e t} \qquad (4)$$

The kinetic results were arrived at based on higher r^2 and low standard deviation (Sd) values. The nonlinear pseudo-first-order and pseudo-second-order plots for AB92 adsorption by CNTs are provided in Figs. 5 and 6 respectively (linear plots are not shown) and the computed results are given in Tables 1 and 2. It is inferred for the previous studies, most of the dye adsorption studies

using activated carbon reported to obey pseudo-second-order kinetics [23–25]. The probable reason may be that the kinetic data is predominantly tested using linear forms of kinetic expressions. In the present study, the results of linear and nonlinear expressions are compared. The results indicate that the nonlinear analysis using the curve fit method generates results with high r^2 and low Sd. Among the two kinetic models, the pseudo-first-order kinetics for the adsorption of AB92 using MWCNT-B, MWCNT-BN and MWCNT-BNS show high r^2 (0.9940 < r^2 < 0.9999) and low Sd (0.131 < Sd < 3.685) under the given range of AB92 concentrations and temperature. Based on high r^2 and low Sd, it is inferred that the AB92 sorption by MWCNT's
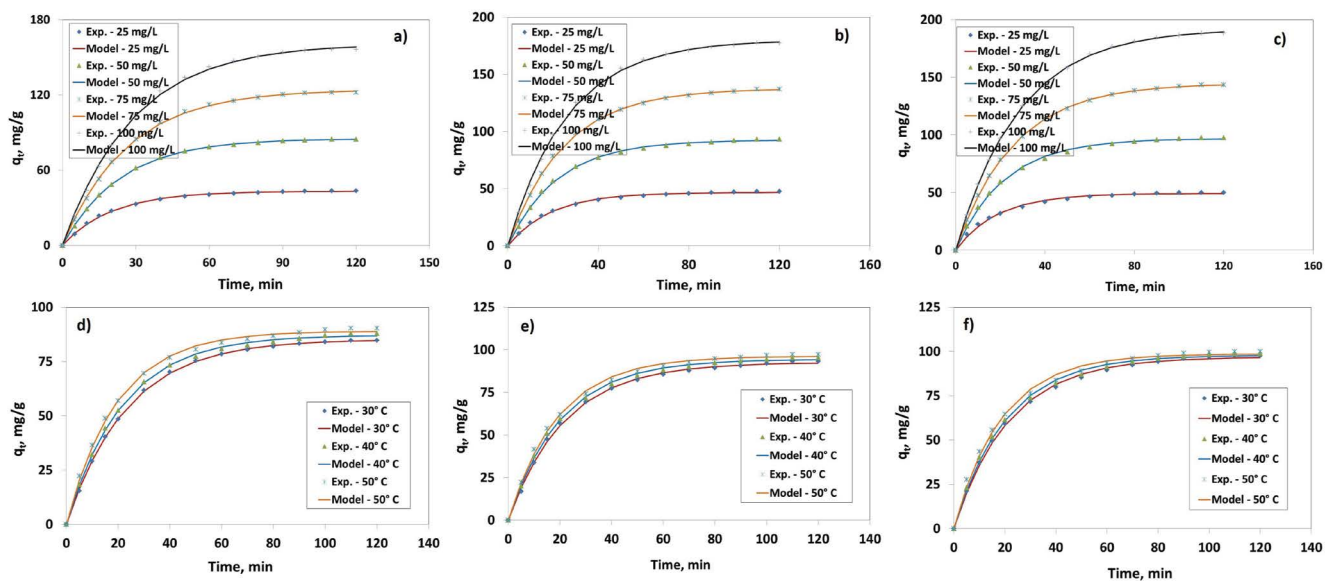

Fig. 5. Nonlinear pseudo-first-order plot at various concentrations (a) MWCNT-B, (b) MWCNT-BN, (c) MWCNT-BNS and at various temperatures (d) MWCNT-B, (e) MWCNT-BN and (f) MWCNT-BNS.
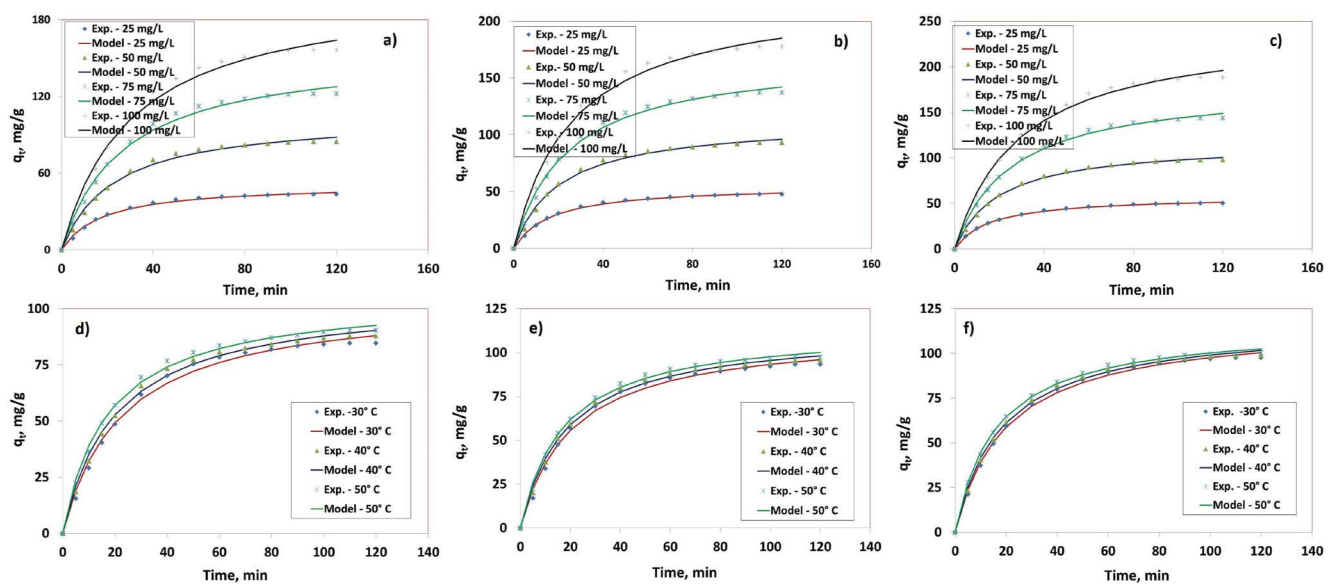

Fig. 6. Nonlinear pseudo-second-order plot at various concentrations (a) MWCNT-B, (b) MWCNT-BN, (c) MWCNT-BNS and at various temperatures (d) MWCNT-B, (e) MWCNT-BN and (f) MWCNT-BNS.

Table 1
Results of linear and nonlinear kinetic analysis at various AB92 concentrations

Adsorbent	Parameters	Linear models				Nonlinear models			
		Initial dye concentration (mg L^{-1})							
		25	50	75	100	25	50	75	100
Pseudo-first-order kinetics									
	$q_{e,exp}$ (mg g^{-1})	43.55	84.68	121.98	156.30	43.55	84.68	121.98	156.30
	$k_1 \times 10^{-2}$ (min^{-1})	2.4412	2.2339	2.0957	1.8194	4.970	4.240	3.793	3.449
MWCNT-B	$q_{e,cal}$ (mg g^{-1})	39.38	79.63	122.94	160.66	43.14	85.23	124.30	160.94
	r^2	0.951	0.9545	0.9627	0.9564	0.9985	0.9998	0.9996	0.9991
	Sd	1.317	1.595	0.305	1.377	0.131	0.175	0.733	1.466
	$q_{e,exp}$ (mg g^{-1})	47.58	93.23	137.10	177.40	47.58	93.23	137.10	177.40
	$k_1 \times 10^{-2}$ (min^{-1})	3.3163	3.1091	3.0630	2.8097	5.261	4.582	4.065	3.811
MWCNT-BN	$q_{e,cal}$ (mg g^{-1})	39.79	80.57	126.82	163.23	46.72	92.49	137.70	180.20
	r^2	0.9787	0.9788	0.9866	0.9785	0.9975	0.9988	0.9992	0.9991
	Sd	2.463	4.001	3.250	4.481	0.271	0.231	0.191	0.886
	$q_{e,exp}$ (mg g^{-1})	50.00	97.58	143.41	188.24	50.00	97.58	143.41	188.24
	$k_1 \times 10^{-2}$ (min^{-1})	5.1360	4.8130	4.1910	4.4680	5.36	4.60	3.88	3.51
MWCNT-BNS	$q_{e,cal}$ (mg g^{-1})	49.77	102.09	149.93	222.95	49.18	96.88	144.75	192.30
	r^2	0.9758	0.9844	0.9977	0.9861	0.9940	0.9985	0.9998	0.9999
	Sd	0.072	1.427	2.064	10.977	0.258	0.220	0.425	1.286
Pseudo-second-order kinetics									
	$q_{e,exp}$ (mg g^{-1})	43.55	84.68	121.98	156.30	43.55	84.68	121.98	156.30
	$k_2 \times 10^{-4}$ (g mg^{-1} min^{-1})	20.39	5.77	3.37	2.15	10.789	4.239	2.427	1.602
MWCNT-B	$q_{e,cal}$ (mg g^{-1})	49.02	99.01	144.93	192.31	51.56	104.62	155.73	205.50
	r^2	0.9866	0.9791	0.9711	0.9604	0.9951	0.9933	0.9925	0.9919
	Sd	1.730	4.532	7.257	11.386	2.532	6.307	10.674	15.559
	$q_{e,exp}$ (mg g^{-1})	47.58	93.23	137.10	177.40	47.58	93.23	137.10	177.40
	$k_2 \times 10^{-4}$ (g mg^{-1} min^{-1})	14.84	5.84	3.20	2.25	10.937	4.399	2.441	1.679
MWCNT-BN	$q_{e,cal}$ (mg g^{-1})	52.91	106.38	161.29	212.77	55.31	112.14	170.46	225.78
	r^2	0.99	0.9817	0.9731	0.9698	0.9972	0.9940	0.9931	0.9914
	Sd	1.685	4.161	7.650	11.184	2.445	5.981	10.550	15.300
	$q_{e,exp}$ (mg g^{-1})	50.00	97.58	143.41	188.24	50.00	97.58	143.41	188.24
	$k_2 \times 10^{-4}$ (g mg^{-1} min^{-1})	15.27	5.96	3.06	1.95	11.25	4.126	2.004	1.924
MWCNT-BNS	$q_{e,cal}$ (mg g^{-1})	55.25	111.11	169.49	227.27	57.82	116.91	179.88	243.68
	r^2	0.9918	0.9863	0.9774	0.9685	0.9991	0.9977	0.9963	0.9954
	Sd	1.660	4.279	8.249	12.345	2.474	6.111	11.534	17.533

follow pseudo-first-order kinetics and the rate of adsorption predominantly depends upon the AB92 concentration. It is also proved that, analysis of adsorption kinetics using nonlinear expressions generate error free results.

3.4. Adsorption isotherms

The adsorption isotherm analysis is very much useful to understand the actual interaction between the AB92 dye with CNT surface and also the mechanism of adsorption [26]. The isotherm data of AB92 adsorption is tested using Langmuir and Freundlich adsorption isotherm models [27,28]. The Langmuir model is derived with an assumption of monolayer distribution of adsorbates and there is no interaction between the adsorbed dye molecules at different sites [29]. The linear and nonlinear form of Langmuir isotherm models are given as follows

$$\text{Linear form: } \frac{C_e}{q_e} = \frac{1}{Q_0 b_L} + \frac{C_e}{Q_0} \tag{5}$$

$$\text{Nonlinear form: } q_e = \frac{Q_0 b_L C_e}{(1 + b_L C_e)} \tag{6}$$

where C_e and q_e are the equilibrium AB92 concentration (mg L^{-1}) and equilibrium adsorption capacity (mg g^{-1}) of selected adsorbents respectively. The unknown parameters b_L (Langmuir rate constant, L mg^{-1}) and Q_0 (Langmuir

Table 2
Results of linear and nonlinear kinetic analysis at various temperatures

Adsorbent	Parameters	Linear models			Nonlinear models		
		Temperature (°C)					
		30	40	50	30	40	50
Pseudo-first-order kinetics							
	$q_{e,\exp}$ (mg g^{-1})	84.68	87.90	90.32	84.68	87.90	90.32
	$k_1 \times 10^{-2}$ (min^{-1})	4.6751	4.1684	3.9151	4.2414	4.6030	5.1267
MWCNT-B	$q_{e,\text{cal}}$ (mg g^{-1})	91.98	84.45	81.13	85.22	87.18	89.03
	r^2	0.9906	0.9893	0.9815	0.9998	0.9993	0.9983
	Sd	2.310	1.091	2.906	0.172	0.229	0.409
	$q_{e,\exp}$ (mg g^{-1})	93.23	95.48	97.40	93.23	95.48	97.40
	$k_1 \times 10^{-2}$ (min^{-1})	4.1915	4.1454	4.3757	4.5818	4.8840	5.1844
MWCNT-BN	$q_{e,\text{cal}}$ (mg g^{-1})	89.17	87.28	89.33	92.49	94.41	96.19
	r^2	0.9965	0.996	0.998	0.9988	0.9987	0.9979
	Sd	1.284	2.595	2.552	0.231	0.338	0.382
	$q_{e,\exp}$ (mg g^{-1})	97.58	98.93	100.00	97.58	98.93	100.00
	$k_1 \times 10^{-2}$ (min^{-1})	4.0763	4.2145	4.7442	4.6016	4.8783	5.3413
MWCNT-BNS	$q_{e,\text{cal}}$ (mg g^{-1})	91.58	94.10	97.79	96.88	97.96	98.69
	r^2	0.9758	0.9844	0.9977	0.9985	0.9978	0.9952
	Sd	1.898	1.527	0.698	0.220	0.308	0.416
Pseudo-second-order kinetics							
	$q_{e,\exp}$ (mg g^{-1})	84.68	87.90	90.32	84.68	87.90	90.32
	$k_2 \times 10^{-4}$ (g mg^{-1} min^{-1})	5.7731	6.5317	7.6810	4.2459	4.7476	5.5431
MWCNT-B	$q_{e,\text{cal}}$ (mg g^{-1})	99.01	100.00	101.01	104.57	105.41	105.70
	r^2	0.9791	0.9853	0.99	0.9932	0.9956	0.9970
	Sd	4.532	3.826	3.380	6.291	5.538	4.863
	$q_{e,\exp}$ (mg g^{-1})	93.23	95.48	97.40	93.23	95.48	97.40
	$k_2 \times 10^{-4}$ (g mg^{-1} min^{-1})	5.8439	6.5722	7.1912	4.3992	4.8171	5.2213
MWCNT-BN	$q_{e,\text{cal}}$ (mg g^{-1})	106.38	107.53	108.70	112.14	113.06	114.01
	r^2	0.9817	0.9871	0.9896	0.9940	0.9962	0.9971
	Sd	4.161	3.808	3.572	5.981	5.558	5.253
	$q_{e,\exp}$ (mg g^{-1})	97.58	98.93	100.00	97.58	98.93	100.00
	$k_2 \times 10^{-4}$ (g mg^{-1} min^{-1})	6.0979	6.4294	7.1137	4.3201	4.7026	5.4302
MWCNT-BNS	$q_{e,\text{cal}}$ (mg g^{-1})	109.89	112.36	114.94	116.91	117.01	116.09
	r^2	0.9918	0.9863	0.9774	0.9977	0.9980	0.9986
	Sd	3.893	4.247	4.725	6.111	5.718	5.087

monolayer adsorption capacity, mg g^{-1}) are evaluated separately using linear and nonlinear mathematical models. The nonlinear Langmuir plots of AB92 adsorption onto the selected adsorbents are shown in Fig. 7a–c and the evaluated results are presented in Table 3.

The maximum Langmuir monolayer adsorption capacity calculated using nonlinear model was found to be 160.53 to 155.18, 146.09 to 144.61 and 117.31 to 104.35 for MWCNT-B, MWCNT-BN and MWCNT-BNS respectively. The Langmuir rate constant evaluated through nonlinear model was found to be 4.35×10^{-2} to 7.98×10^{-2}, 0.1463 to 0.2975 and 0.5094 to 1.1454 L mg^{-1}, respectively for MWCNT-B, MWCNT-BN and MWCNT-BNS. It was observed that the selected adsorbents MWCNT-B, MWCNT-BN and

MWCNT-BNS show comparable adsorption capacity with that of adsorbents reported in the literature.

Another widely used and one of the oldest isotherm models is Freundlich adsorption isotherm [28]. This isotherm is derived based on the assumption of unevenly distributed adsorption sites. The linear and nonlinear form of Freundlich adsorption isotherm is given as follows:

$$\text{Linear form: } \log q_e = \log k_f + \frac{1}{n}\log C_e \tag{7}$$

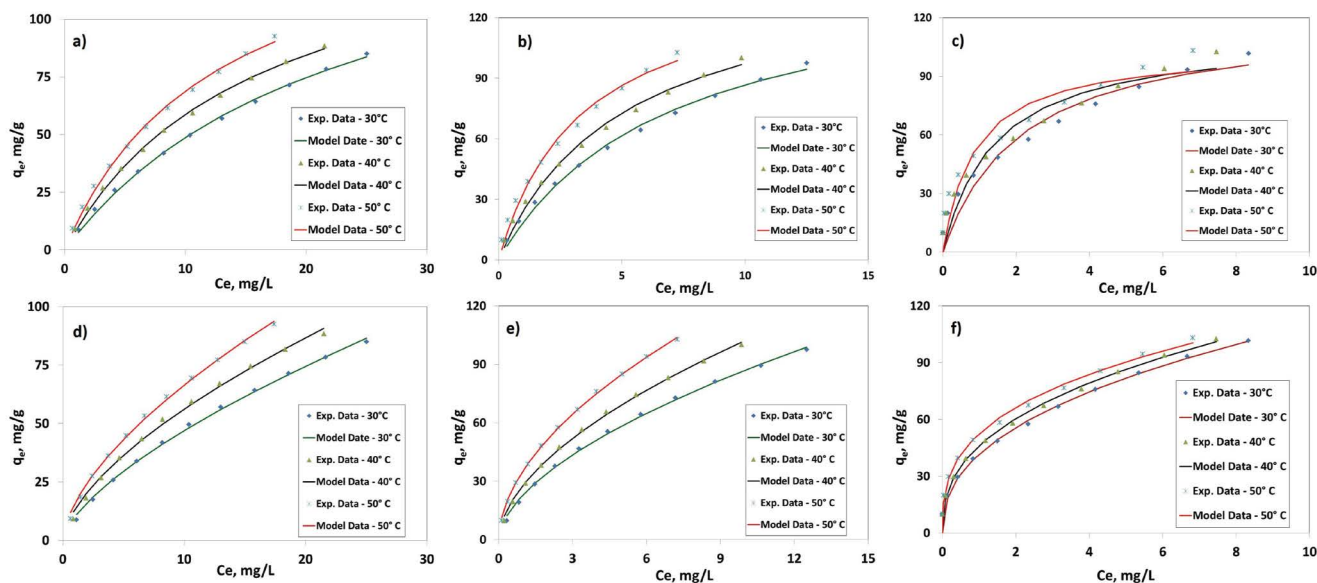$$\text{Nonlinear form: } q_e = k_f C_e^{1/n} \tag{8}$$

Fig. 7. Nonlinear Langmuir plot (a) MWCNT-B, (b) MWCNT-BN, (c) MWCNT-BNS and nonlinear Freundlich plots (d) MWCNT-B, (e) MWCNT-BN and (f) MWCNT-BNS.

Table 3
Results of isotherm analysis for AB92 adsorption

Adsorbent	Parameter	Linear model			Nonlinear model		
		Temperature (°C)					
		30	40	50	30	40	50
Langmuir isotherm							
MWCNT-B	Q_0 (mg g^{-1})	147.06	142.86	140.85	160.53	150.20	155.18
	b_L (L mg^{-1})	0.0060	0.0064	0.0066	0.0435	0.0643	0.0798
	r^2	0.9835	0.99	0.9798	0.9982	0.9982	0.9961
	Sd	–	–	–	1.126	1.165	1.805
MWCNT-BN	Q_0 (mg g^{-1})	107.53	105.26	103.09	146.00	146.09	144.61
	b_L (L mg^{-1})	0.0092	0.0094	0.0096	0.1463	0.1987	0.2975
	r^2	0.9489	0.9552	0.9524	0.9938	0.9922	0.9871
	Sd	–	–	–	2.426	2.783	3.685
MWCNT-BNS	Q_0 (mg g^{-1})	107.53	105.26	103.09	117.31	111.99	104.35
	b_L (L mg^{-1})	0.0092	0.0094	0.0096	0.5094	0.7053	1.1454
	r^2	0.9489	0.9552	0.9524	0.9467	0.9354	0.9055
	Sd	–	–	–	7.406	8.222	10.013
Freundlich isotherm							
MWCNT-B	n	1.387	1.434	1.472	1.503	1.598	1.606
	k_f (mg$^{1-1/n}$ L$^{1/n}$ g^{-1})	8.823	11.264	14.064	32.6	62.4	84.5
	r^2	0.996	0.9926	0.9945	0.9998	0.9997	0.9998
	Sd	–	–	–	0.352	0.516	0.385
MWCNT-BN	n	2.499	2.726	3.305	1.742	1.783	1.845
	k_f (mg$^{1-1/n}$ L$^{1/n}$ g^{-1})	42.628	47.250	53.926	239.3	382.7	725.6
	r^2	0.9977	0.9966	0.9902	0.9998	0.9999	0.9999
	Sd	–	–	–	0.410	0.377	0.253
MWCNT-BNS	n	2.499	2.726	3.305	2.387	2.565	2.963
	k_f (mg$^{1-1/n}$ L$^{1/n}$ g^{-1})	42.628	47.250	53.926	73.80	186.58	1254.84
	r^2	0.9977	0.9966	0.9902	0.9989	0.9989	0.9986
	Sd	–	–	–	1.055	1.082	1.214

where k_f is the Freundlich adsorption constant and n is a parameter related to adsorption intensity. The nonlinear Freundlich plots are shown in Fig. 7d–f and the calculated Freundlich parameters are provided in Table 3. The Freundlich constant related to adsorption capacity calculated from nonlinear plot varied from 32.6 to 84.5, 293.3 to 725.6 and 738.0 to 1,254.8 mg$^{1-1/n}$ L$^{1/n}$ g^{-1} for MWCNT-B, MWCNT-BN and MWCNT-BNS respectively. Similarly the parameter related to adsorption intensity varied from 1.508 to 1.606, 1.742 to 1.845 and 2.387 to 2.963 for MWCNT-B, MWCNT-BN and MWCNT-BNS respectively. For any adsorption system with n value between 1 and 10, the adsorption is favourable and proceeds with good ease. In-depth analysis of the results obtained from linear and nonlinear plots proved that the nonlinear analysis using curve fit method yielded accurate results with low Sd values and high r^2 values.

The applicability of nonlinear curve fit analysis is also supported by high r^2_{adj} and high reduced chi square values. From the isotherm analysis it may be concluded that Freundlich adsorption isotherm is more appropriate to describe the adsorption dynamics of AB92 by MWCNT-B, MWCNT-BN and MWCNT-BNS. The suitability of Freundlich adsorption isotherm substantiated that the adsorption of AB92 onto MWCNT-B, MWCNT-BN and MWCNT-BNS proceeds through an energetically heterogeneous surface along with multilayer adsorption. Similar trend of adsorption was observed by Sismanoglu et al. [23], for Reactive Red 195 (RR195) and Reactive Blue 21 (RB21) dye adsorption by clinoptilolite adsorbent.

3.5. Mechanism of adsorption

The intraparticle diffusion model gives some useful information about the mechanism of adsorption. The intraparticle diffusion model proposed by Weber and Morris is given as follows:

$$q_t = k_{id}t^{1/2} \tag{9}$$

where k_{id} represents the intraparticle diffusion rate constant [30]. The adsorption data of AB92 onto MWCNT-B, MWCNT-BN and MWCNT-BNS are analyzed using the intraparticle diffusion model (figure not shown) and the k_{id} calculated from the slope of second linear portion are given in Table 4. The plot of q_t vs. $t^{1/2}$ is a multi-linear plot and it indicates that AB92 adsorption onto the selected adsorbents occurred in three phases. The initial portion with highest slope indicates the film diffusion occurring on the adsorbents surface. The progress of intra-particle or pore diffusion is represented by the second-linear portion. This step is the slowest and is responsible for rate limiting. The third-linear portion is due to the final equilibrium adsorption. The multi-linear plot substantiates that more than one type of mechanism is responsible for the adsorption of AB92 on to MWCNT-B, MWCNT-BN and MWCNT-BNS adsorbents [31]. Based on the plot, second-step is more predominant and intraparticle diffusion mechanism plays a notable role in the present adsorption system [32].

The intraparticle diffusion rate constant k_{id} decreased from 0.644 to 0.114, 0.529 to 0.119 and 0.542 to 0.122 mg g^{-1} min$^{-1/2}$ respectively for MWCNT-B, MWCNT-BN and MWCNT-BNS adsorbents on increasing the AB92 concentration from 25 to 100 mg L^{-1}. The same constant increases from 0.285 to 0.317, 0.266 to 0.324 and 0.272 to 0.315 mg g^{-1} min$^{-1/2}$ respectively for MWCNT-B, MWCNT-BN and MWCNT-BNS on increasing the temperature from 30°C to 50°C. The film and pore diffusion of AB92 onto doped MWCNTs proceeds through any of the following pathways.

- The film diffusion occurs on the entire curved high surface area MWCNTs also the defects and active sites helps for enhanced surface adsorption.
- The MWCNT bundles create some interstitial channels; these sites are highly useful for the adsorption through pore diffusion.
- The grooves created at the periphery of the junction between two adjacent tubes are also useful for adsorption through diffusion [33].

3.6. Thermodynamics of adsorption

It is essential to evaluate the thermodynamic parameters like Gibbs free energy, enthalpy ($\Delta H°$) and entropy ($\Delta S°$) of adsorption. These parameters were evaluated using the following expressions:

$$\Delta G° = RT\ln\left(55.5 \times b_L\right) \tag{10}$$

$$\ln\left(b_L \times 55.5\right) = \frac{\Delta S°}{R} - \frac{\Delta H°}{RT} \tag{11}$$

Table 4
Results of intraparticle diffusion model

Adsorbent	Parameter	AB92 concentrations (mg L^{-1})				Temperature (°C)		
		25	50	75	100	30	40	50
MWCNT-B	k_{id} (mg g^{-1} min$^{-1/2}$)	0.644	0.285	0.166	0.114	0.285	0.304	0.317
	r^2	0.9869	0.9831	0.9797	0.9709	0.9831	0.9768	0.9818
MWCNT-BN	k_{id} (mg g^{-1} min$^{-1/2}$)	0.529	0.266	0.149	0.119	0.266	0.284	0.324
	r^2	0.984	0.9855	0.9836	0.979	0.9855	0.9819	0.9805
MWCNT-BNS	k_{id} (mg g^{-1} min$^{-1/2}$)	0.542	0.272	0.172	0.122	0.272	0.300	0.315
	r^2	0.9957	0.9913	0.97	0.9853	0.9913	0.9687	0.9795

According to Liu [34], the Langmuir constant must be multiplied with molarity of water (1000 g divided by molecular weight of water) to get errorless Gibbs free energy. The thermodynamic parameters of AB92 adsorption are calculated based on the Van't Hoff's plot (figure not shown). The negative Gibbs free energy in kJ mol^{-1} (–2.22 to –3.87 for MWCNT-B, –5.28 to –7.30 for MWCNT-BN and 8.42 to 10.81 for MWCNT-BNS) indicates that the adsorption of AB92 is spontaneous and favourable.

Among the three adsorbents, (24.72 kJ mol^{-1} for MWCNT-B, 28.82 kJ mol^{-1} for MWCNT-BN and 32.89 kJ mol^{-1} for MWCNT-BNS) showed high positive enthalpy, indicates that, increase of temperature creates more suitable environment for AB92 adsorption. The enthalpy values greater than 20 kJ mol^{-1} indicated that the adsorption is more of chemisorptions rather than physisorption [35]. The entropy of adsorption (J K^{-1} mol^{-1}) for AB92 adsorption by the selected adsorbents is positive and increases from MWCNT-B (89.13) < MWCNT-BN (112.36) < MWCNT-BNS (136.08). Increased randomness at the solid liquid interface is substantiated by the positive value of $\Delta S°$ [36].The Gibbs free energy is more negative for MWCNT-BNS, which substantiated that the adsorption of AB92 onto MWCNT-BNS is more favourable than MWCNT-BN and MWCNT-B. For all the three adsorbents, increase in temperature favours the AB92 adsorption. The endothermic nature of AB92 adsorption is substantiated from the positive sign of $\Delta H°$ for all the three selected adsorbents.

3.7. Recyclability studies

Desorption studies are also performed to evaluate the nature of eluent required for the maximum desorption. All the three adsorbents show an increase in desorption with increase of pH. Highest desorption achieved at a pH of 12 and it was found to be 83.4% for MWCNT-B, 80.3% for MWCNT-BN and 79.2% for MWCNT-BNS. The adsorbents are also tested for their recyclability through repeated adsorption and desorption studies using the spent adsorbents. The recyclability studies substantiated that MWCNT-B can adsorb more the 90% of AB92 upto 4 cycles, MWCNT-BN can adsorb more than 90% up to 5 cycles and MWCNT-BNS show excellent recyclability of more 90% adsorption up to 7 cycles. The prepared adsorbents are undoubtedly potential adsorbents for anionic acid dye adsorptions. Among the three prepared nano-adsorbents, MWCNT-BNS show superior adsorption characteristics with the highest number of recycles. According to Fu et al., the high removal characteristics of BNS doped MWCNT is due to π–π mounding interactions between the MWCNT's surface with AB92 dye [37].

4. Conclusion

The present study explored the functionalization of carbon nanotubes derived from plant based carbon source and its application as adsorbent. The characterization revealed that the thickness of functionalized carbon nanotubes were in the range 50–60 nm, the inter planar distance of layers was 0.35 nm and the I$_D$/I$_G$ ratio calculated for the materials were in the range 0.6–1.2. The study indicated that

the functionalized carbon nanotubes surface was rather smooth however; it retained their structure probably due to the intact inner layers. Kinetics of adsorption under various concentrations and temperatures are evaluated using linear and nonlinear mathematical models. The Gibbs free energy is more negative for MWCNT-BNS (–10.81 kJ mol^{-1}), which substantiated that the adsorption of AB92 onto MWCNT-BNS is more favourable than MWCNT-BN and MWCNT-B. The recyclability of adsorbents showed that up to 90% of initial dye concentration was removed for 7 cycles. The prepared adsorbents are undoubtedly potential adsorbents for anionic acid dye adsorptions. Among the three prepared adsorbents, MWCNT-BNS shows superior adsorption characteristics at pH 6, with mass of adsorption 1.995 mg g^{-1} min^{-1} following pseudo-first-order kinetics and with highest number of recycles.

References

[1] K.S. Ibrahim, Carbon nanotubes-properties and applications: a review, Carbon Lett., 14 (2013) 131–144.
[2] I.M. Jauris, S.B. Fagan, M.A. Adebayo, F.M. Machado, Adsorption of Acridine Orange and methylene blue synthetic dyes and anthracene on single wall carbon nanotubes: a first principle approach, Comput. Theor. Chem., 1076 (2016) 42–50.
[3] Y. Rangraz, M.M. Heravi, Recent advances in metal-free heteroatom-doped carbon heterogonous catalysts, RSC Adv., 11 (2021) 23725–23778.
[4] S. Liu, G. Li, Y. Gao, Z. Xiao, J. Zhang, Q. Wang, X. Zhang, L. Wang, Doping carbon nanotubes with N, S, and B for electrocatalytic oxygen reduction: a systematic investigation on single, double, and triple doped modes, Catal. Sci. Technol., 7 (2017) 4007–4016.
[5] U. Kamran, S.J. Park, Microwave-assisted acid functionalized carbon nanofibers decorated with Mn doped TNTs nanocomposites: efficient contenders for lithium adsorption and recovery from aqueous media, J. Ind. Eng. Chem., 92 (2020) 263–277.
[6] V. Kumar, P. Saharan, A.K. Sharma, A. Umar, I. Kaushal, A. Mittal, Y. Al-Hadeethi, B. Rashad, Silver doped manganese oxide-carbon nanotube nanocomposite for enhanced dye-sequestration: isotherm studies and RSM modelling approach, Ceram. Int., 46 (2020) 10309–10319.
[7] D. Zhao, Y. Ding, S. Chen, T. Bai, Y. Ma, Adsorption of Methylene blue on carbon nanotubes from aqueous solutions, Asian J. Chem., 25 (2013) 5756–5758.
[8] J. Mittal, Permissible synthetic food dyes in India, Reson. – J. Sci. Educ., 25 (2020) 567–577
[9] K. Rehman, T. Shahzad, A. Sahar, S. Hussain, F. Mahmood, M.H. Siddique, M.A. Siddique, M.I. Rashid, Effect of Reactive black 5 azo dye on soil processes related to C and N cycling, PeerJ, 6 (2018) e4802, doi: 10.7717/peerj.4802
[10] B. Lellis, C.Z. Fávaro-Polonio, J.A. Pamphile, J.C. Polonio, Effects of textile dyes on health and the environment and bioremediation potential of living organisms, Biotech. Res. Innov., 3 (2019) 275–290.
[11] B. Murugesan, A. Sivakumar, A. Loganathan, P. Sivakumar, Synthesis and photocatalytic studies of lanthanum oxide doped nano carbon hollow spheres, J. Taiwan Inst. Chem. Eng., 71 (2017) 364–372.
[12] U. Kamran, H.N. Bhatti, S. Noreen, M.A. Tahir, S.J. Park, Chemically modified sugarcane bagasse-based biocomposites for efficient removal of Acid red 1 dye: kinetics, isotherms,

thermodynamics, and desorption studies, Chemosphere, 291 (2022) 132796, doi: 10.1016/j.chemosphere.2021.132796.

[13] U. Kamran, H.N. Bhatti, M. Iqbal, S. Jamil, M. Zahid, Biogenic synthesis, characterization and investigation of photocatalytic and antimicrobial activity of manganese nanoparticles synthesized from *Cinnamomum verum* bark extract, J. Mol. Struct., 1179 (2019) 532–539.

[14] E. Kanagaraj, P. Mahalingam, R. Siddharthan, P. Sivakumar, Growth of multi-walled carbon nanotubes along with gravity by spray pyrolysis of natural precursor, Rasayan J. Chem., 14 (2021) 2311–2317.

[15] M. Abha, T. Pawan, R. Padmnabh, M. Devi, FTIR spectroscopy of multi-walled carbon nanotubes: a simple approach to study the nitrogen doping, J. Nanosci. Nanotechnol., 7 (2007) 1820–1823.

[16] F. Leiyu, Z. Qin, H. Yujun, P. Kangshou, W. Feng, Y. Yuanyuan, C. Yinguang, Boron-, sulfur-, and phosphorus-doped graphene for environmental applications, Sci. Total Environ., 698 (2019) 134239, doi: 10.1016/j.scitotenv.2019.134239.

[17] G. Keru, P.G. Ndungu, V.O. Nyamori, Effect of boron concentration on physicochemical properties of borondoped carbon nanotubes, Mater. Chem. Phys., 153 (2015) 323–332.

[18] P.N. Palanisamy, P. Sivakumar, Kinetic and isotherm studies of the adsorption of Acid blue 92 using a low-cost non-conventional activated carbon, Desalination, 249 (2009) 388–397.

[19] R. Aravindhan, N.N. Fathima, J.R. Rao, B.U. Nair, Equilibrium and thermodynamic studies on the removal of basic black dye using calcium alginate beads, Colloids Surf., A, 299 (2007) 232–238.

[20] É.C. Lima, M.A. Adebayo, F.M. Machado, Chapter 3 – Kinetic and Equilibrium Models of Adsorption, C.P. Bergmann, F.M. Machado, Eds., Carbon Nanomaterials as Adsorbents for Environmental and Biological Applications, Springer, 2015, pp. 33–69, doi: 10.1007/978-3-319-18875-1_3.

[21] S. Lagergren, About the theory of so-called adsorption of soluble substances, Kung Sven Veten Hand, 24 (1898) 1–39.

[22] Y.S. Ho, G. McKay, Pseudo-second-order model for sorption processes, Process Biochem., 34 (1999) 451–465.

[23] T. Sismanoglu, Y. Kismir, S. Karakus, Single and binary adsorption of reactive dyes from aqueous solutions onto clinoptilolite, J. Hazard Mater., 184 (2010) 164–169.

[24] M. Hani, S. Mahmoud, Adsorption of Reactive red 195 dye from industrial wastewater by dried soybean leaves modified with acetic acid, Desal. Water Treat., 178 (2020) 312–321.

[25] O. Aksakal, H. Ucun, Equilibrium, kinetic and thermodynamic studies of the biosorption of textile dye (Reactive red 195) onto *Pinus sylvestris* L, J. Hazard. Mater., 181 (2010) 666–672.

[26] P. Ashokan, M. Asaithambi, V. Sivakumar, P. Sivakumar, Batch and column mode adsorption studies of Reactive red 195 dye using *Adenanthera paronina* L seed activated carbon, Groundwater Sustainable Dev., 15 (2021) 100671, doi: 10.1016/j.gsd.2021.100671.

[27] I. Langmuir, The constitution and fundamental properties of solids and liquids. II. Liquids, J. Am. Chem. Soc., 39 (1917) 1848–1906.

[28] H. Freundlich, Über die Adsorption in Lösungen, Z. Phys. Chem., 57U (1907) 385–470.

[29] M. Hosseinzehi, M. Khatebasreh, A. Dalvand, Modeling of Reactive black 5 azo dye adsorption from aqueous solution on activated carbon prepared from poplar sawdust using response surface methodology, Int. J. Environ. Anal. Chem., (2020), doi: 10.1080/03067319.2020.1819991.

[30] J. Weber, J.C. Morris, Kinetics of adsorption on carbon from solution, J. Sanit. Eng. Div., 89 (1963) 31–60.

[31] V. Kumaravelan, P. Sivakumar, Fe_3O_4 immobilized magnetic nano carbon balls for the adsorption of methylene blue dye in batch and packed bed column mode, Desal. Water Treat., 115 (2018) 288–299.

[32] H.K. Boparai, M. Joseph, D.M. O'Carroll, Kinetics and thermodynamics of cadmium ion removal by adsorption onto nano zerovalent iron particles, J. Hazard. Mater., 186 (2011) 458–465.

[33] C. Fernando, E. Isabel, A. Sandeep, M. Erich, A molecular simulation study of propane and propylene adsorption onto single-walled carbon nanotube bundles, J. Nanosci. Nanotechnol., 10 (2010) 2537–2546.

[34] Y. Liu, Is the free energy change of adsorption correctly calculated?, J. Chem. Eng. Data, 54 (2009) 1981–1985.

[35] S.K. Theydan, M.J. Ahmed, Adsorption of methylene blue onto biomass-based activated carbon by $FeCl_3$ activation: equilibrium, kinetics, and thermodynamic studies, J. Anal. Appl. Pyrolysis, 97 (2012) 116–122.

[36] F. Çiçek, D. Özer, A. Özer, A. Özer, Low cost removal of reactive dyes using wheat bran, J. Hazard. Mater., 146 (2007) 408–416.

[37] J. Fu, Z. Chen, M. Wang, S. Liu, J. Zhang, J. Zhang, R. Han, Q. Xu, Adsorption of methylene blue by a high-efficiency adsorbent (polydopamine microspheres): kinetics, isotherm, thermodynamics and mechanism analysis, Chem. Eng. J., 259 (2015) 53–61.